Article

Pyrolysis, Crystallization, and Sintering of Mesostructured Titania Thin Films Assessed by in Situ Thermal Ellipsometry

John D. Bass, David Grosso, Ce#dric Boissiere, and Cle#ment Sanchez

J. Am. Chem. Soc., **2008**, 130 (25), 7882-7897 • DOI: 10.1021/ja078140x • Publication Date (Web): 29 May 2008

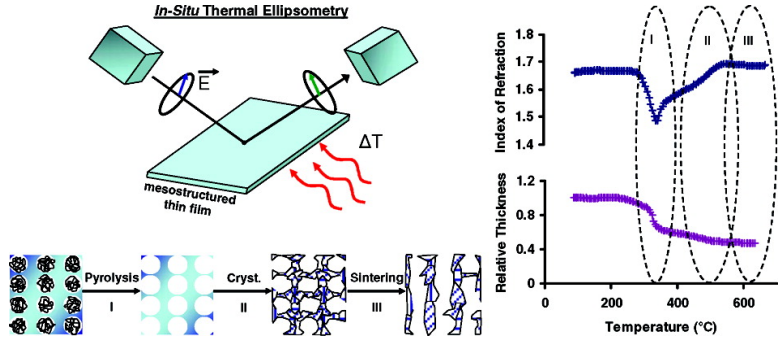

More About This Article

Additional resources and features associated with this article are available within the HTML version:

- Supporting Information
- Links to the 1 articles that cite this article, as of the time of this article download
- Access to high resolution figures
- Links to articles and content related to this article
- Copyright permission to reproduce figures and/or text from this article

View the Full Text HTML

J|A|C|S
ARTICLES

Published on Web 05/29/2008

Pyrolysis, Crystallization, and Sintering of Mesostructured Titania Thin Films Assessed by in Situ Thermal Ellipsometry

John D. Bass, David Grosso,* Cédric Boissiere, and Clément Sanchez

Laboratoire de Chimie de la Matière Condensée de Paris, Université Pierre et Marie Curie-Paris 6 and CNRS, 4 place Jussieu, 75252 Paris 05, France

Received October 30, 2007; E-mail: david.grosso@upmc.fr

Abstract: In-situ thermal ellipsometric analysis is used to elucidate new and fine-scale details on the thermally driven densification, pyrolysis, crystallization, and sintering of dense and ordered mesoporous titania thin films prepared by evaporation-induced self-assembly. The role of the heating schedule, initial film thickness, nature of the substrate and templating agent, solution aging, and presence of water and other additives in the calcination environment is examined. Each of these parameters is shown to have unique and often substantial effects on the final film structure, while the technique itself provides detailed insight into the chemical origin and evolution of these effects. In-situ monitoring and control over the governing chemical processes, such as high-temperature adsorption phenomena that impact nanocrystal growth, is also demonstrated. The evolution of both the porosity and chemical processes occurring inside these materials are evaluated, including extraction of kinetic parameters for the pyrolysis of the template and crystallization of the matrix walls. The latter is shown to be strongly dependent on the presence of mesoscale ordering with ordered cubic films indicating a 1D diffusion-limited crystallization process and dense films following a 3D diffusion-limited process. Less well-ordered mesoporous films, despite similarities in pore volume and pore size distributions, are kinetically more reminiscent of dense films in terms of crystallization. In-situ thermal ellipsometry, by detailing the evolution of the thermally driven chemistry and ceramization that dictate the final film properties, provides immensely important insight into the synthesis and optimization of advanced functional materials based on titania and other metal oxide thin films.

Introduction

Among the library of shapes and morphologies of mesoporous oxide materials developed in recent years, thin films have proved to be highly suitable for integration into a variety of advanced functional applications due to their applicability as coatings and ability to combine high surface areas with a low material footprint. Their use in high-tech domains including photonics,[1] catalysis,[2,3] membranes,[4] biological supports,[5–7] sensing,[8,9] and environmental applications[10] thus remains a subject of spectacular interest today. Key to the preparation of such materials after initial assembly[11] is most often a thermal post-treatment.[12,13] Thermal treatment is by far the most utilized and perhaps the most efficient method for creation of useful porous materials from, for example, organically templated inorganic films,[11] and the chemical evolution of the chemical processes involved strongly dictates the final characteristics of these materials.[12,13]

Thermally driven chemical processes, including dehydration, condensation, densification, decomposition/pyrolysis, crystallization, and sintering, dictate the material stability, porosity, surface area, mesostructure, nature of the chemical properties of the interface, and, in some systems, type, morphology, dimension, and distribution of the nanocrystals composing the matrix walls.[2,12,14–16] Tuned annealing and calcination conditions have routinely been shown to be key in facilitating and maintaining proper control of morphology at the mesoscopic

(1) Baeck, S. H.; Choi, K. S.; Jaramillo, T. F.; Stucky, G. D.; McFarland, E. W. *Adv. Mater.* **2003**, *15* (15), 1269−1273.
(2) Sakatani, Y.; Grosso, D.; Nicole, L.; Boissiere, C.; Soler-Illia, G. J. D. A.; Sanchez, C. *J. Mater. Chem.* **2006**, *16* (1), 77–82.
(3) Martinez-Ferrero, E.; Sakatani, Y.; Boissiere, C.; Grosso, D.; Fuertes, A.; Fraxedas, J.; Sanchez, C. *Adv. Funct. Mater.* **2007**, *17* (16), 3348–3354.
(4) Guliants, V. V.; Carreon, M. A.; Lin, Y. S. *J. Membr. Sci.* **2004**, *235* (1−2), 53–72.
(5) Bass, J. D.; Grosso, D.; Boissiere, C.; Belamie, E.; Coradin, T.; Sanchez, C. *Chem. Mater.* **2007**, *19*, 4349–4356.
(6) Bass, J. D.; Belamie, E.; Grosso, D.; Boissiere, C.; Coradin, T.; Sanchez, C. *J. Biomed. Mat. Res. A*, submitted for publication.
(7) Yan, X. X.; Yu, C. Z.; Zhou, X. F.; Tang, J. W.; Zhao, D. Y. *Angew. Chem., Int. Ed.* **2004**, *43* (44), 5980–5984.
(8) Nicole, L.; Boissiere, C.; Grosso, D.; Hesemann, P.; Moreau, J.; Sanchez, C. M. *Chem. Commun.* **2004**, 2312–2313.
(9) Wirnsberger, G.; Scott, B. J.; Stucky, G. D. *Chem. Commun.* **2001**, 119–120.
(10) Bosc, F.; Edwards, D.; Keller, N.; Keller, V.; Ayral, A. *Thin Solid Films* **2006**, *495* (1−2), 272–279.
(11) Grosso, D.; Cagnol, F.; Soler-Illia, G. J. D. A.; Crepaldi, E. L.; Amenitsch, H.; Brunet-Bruneau, A.; Bourgeois, A.; Sanchez, C. *Adv. Funct. Mater.* **2004**, *14* (4), 309–322.
(12) Grosso, D.; Boissiere, C.; Nicole, L.; Sanchez, C. *J. Sol-Gel Sci. Technol.* **2006**, *40* (2−3), 141–154.
(13) Sanchez, C.; Boissiere, C.; Grosso, D.; Laberty, C.; Nicole, L. *Chem. Mater.* **2008**, in press.
(14) Grosso, D.; Soler-Illia, G. J. D. A.; Crepaldi, E. L.; Cagnol, F.; Sinturel, C.; Bourgeois, A.; Brunet-Bruneau, A.; Amenitsch, H.; Albouy, P. A.; Sanchez, C. *Chem. Mater.* **2003**, *15* (24), 4562–4570.
(15) Crepaldi, E. L.; Soler-Illia, G. J. D. A.; Bouchara, A.; Grosso, D.; Durand, D.; Sanchez, C. *Angew. Chem., Int. Ed.* **2003**, *42* (3), 347−351.
(16) Grosso, D.; Boissiere, C.; Smarsly, B.; Brezesinski, T.; Pinna, N.; Albouy, P. A.; Amenitsch, H.; Antonietti, M.; Sanchez, C. *Nat. Mater.* **2004**, *3* (11), 787–792.

10.1021/ja078140x CCC: $40.75

level, such as in the production of mesoporous films for effective photocatalysis[2,3] or in the synthesis of complex nanocrystalline multimetallic oxide systems.[16] Careful crystallization, for example, is needed to balance precise control of scaffolding and nanocrystal intergrowth for the formation of nanocrystalline walls with the maintenance of mesostructural integrity during diffusive sintering.[12]

Beyond the heating schedule, other factors present during, or prior to, thermal treatment significantly impact the balance of kinetic processes that lead to efficient functional materials. The composition of the initial precursor solution, including chemical evolution of inorganic species caused by aging,[12,15] and the composition of the calcination atmosphere, especially active chemical components including water[17] and mineral acids,[18–20] are known to control material properties. Such influences often emerge from the distribution and stabilization of intermediate metastable nanostructures in the as-synthesized film.[12,15,17]

For films with submicrometer thicknesses, the film thickness and influence of the substrate are also potentially important factors due to substrate diffusional, epitaxial, dilatational, electrical, or magnetic effects. In this regard, film thickness has been shown to be a critical parameter in the design of photoactive devices for instance.[21,22]

Mesoscale organization of thin films is of great interest in terms of how such organization can be used to increase surface area, facilitate access to active sites, perturb physical and chemical processes through confinement effects, and so on.[23] The effect of meso-organization on chemical processes such as crystallization of the matrix walls and the resulting consequences in terms of interfacial chemistry and activity is potentially immensely important in view of the large amount of attention given to the development of highly ordered mesostructured materials.[12,24,25]

For all of these parameters, characterization of chemical processes occurring within the pores, such as pyrolysis of the template, within the matrix, such as densification, crystallization, and sintering, and at the interface, such as absorption, during thermal treatment would greatly facilitate the synthesis and optimization of new ordered mesostructured oxide films for advanced applications. To date, in-situ characterization during thermal treatment has been carried out through simultaneous small- and wide-angle X-ray scattering SAXS/WAXS investigations using a synchrotron radiation source.[14,16] While highly successful, this approach is only sensitive to organizational information and suffers from the limited availability of synchrotron sources. Recently, the use of ellipsometric techniques has emerged to track compositional changes occurring within ordered mesostructured films, specifically in evaluating thicknesses and information on the porous network using environmentally controlled adsorption experiments.[26–28] In-situ thermal ellipsometry has been used to monitor film thickness for sol−gel-derived materials and monitoring phase transformations in sputtered alloys for memory applications.[29,30] Its use in broader contexts, specifically related to mesostructured films and as a tool to parametrically investigate synthesis of such materials, has not, to our knowledge, been investigated.

Here we investigate the use of in-situ thermal ellipsometry in combination with in-situ SAXS, ex-situ IR, and ellipsometry porosimetry to investigate the thermal evolution of dense and mesostructured thin films. Titania films prepared by evaporation-induced self-assembly (EISA) are chosen as model systems since the film formation mechanisms are well characterized and due to their applicability in electron-transfer devices.[2,10,11,14,15,31,32] Through this technique we evaluate the evolution of films in terms of thickness and index of refraction as a function of the processing parameters detailed above. This in turn is used to provide detailed information on the evolution of porosity during the calcination process and give kinetic information on transformations occurring inside the cavities and within the matrix during crystallization. This includes information on the crystallization mechanism as a function of the mesostructuration, from dense, to less-ordered, to highly ordered films.

The results presented here emphasize the kinetic processes during thermal treatment responsible for production of functional materials based on thin-film architectures. These kinetic processes are shown to be dependent on a host of parameters including the heating rate, atmosphere, matrix composition, film−substrate, template, thickness, structure, and ordering. Moreover, this technique is broadly applicable to any thin film system amenable to ellipsometry, whether prepared via dip coating, spray coating, meniscus coating, spin coating, etc. As such, this technique sheds unique, in-situ insight into the interplay of thermally driven physicochemical phenomena leading to functional materials.

Results and Discussion

Thin mesoporous and dense titania films were prepared as described in the Experimental Section and outlined in Scheme 1. They were all obtained by dip-coating solutions made of $TiCl_4$ precursor dispersed into a mixture of H_2O and ethanol. PEO-based block copolymers were added as templates for mesoporous films. After deposition, a humidity treatment was applied before thermal treatment. Deviations from the standard preparation protocol were applied by varying chemical and processing parameters as illustrated in Scheme 1.

In-situ ellipsometry measurements for 82 nm thick dense and a 262 nm thick F127 templated mesostructured titania films heated at a continuous ramp rate of 30 °C/min are shown in

(17) Levchenko, A. A.; Li, G. S.; Boerio-Goates, J.; Woodfield, B. F.; Navrotsky, A. *Chem. Mater.* **2006**, *18* (26), 6324–6332.
(18) Yanagisawa, K.; Ovenstone, J. *J. Phys. Chem. B* **1999**, *103* (37), 7781–7787.
(19) Matthews, A. *Am. Mineral.* **1976**, *61*, 419–424.
(20) Wu, M. M.; Lin, G.; Chen, D. H.; Wang, G. G.; He, D.; Feng, S. H.; Xu, R. R. *Chem. Mater.* **2002**, *14* (5), 1974–1980.
(21) Takahashi, M.; Tsukigi, K.; Uchino, T.; Yoko, T. *Thin Solid Films* **2001**, *388* (1−2), 231–236.
(22) Tada, H.; Tanaka, M. *Langmuir* **1997**, *13* (2), 360–364.
(23) Carreon, M. A.; Choi, S. Y.; Mamak, M.; Chopra, N.; Ozin, G. A. *J. Mater. Chem.* **2007**, *17* (1), 82–89.
(24) Zhao, D. Y.; Yang, P. D.; Margolese, D. I.; Chmelka, B. F.; Stucky, G. D. *Chem. Commun.* **1998**, 2499–2500.
(25) Lu, Y. F.; Ganguli, R.; Drewien, C. A.; Anderson, M. T.; Brinker, C. J.; Gong, W. L.; Guo, Y. X.; Soyez, H.; Dunn, B.; Huang, M. H.; Zink, J. I. *Nature* **1997**, *389* (6649), 364–368.
(26) Boissiere, C.; Grosso, D.; Lepoutre, S.; Nicole, L.; Bruneau, A. B.; Sanchez, C. *Langmuir* **2005**, *21* (26), 12362–12371.
(27) de Theije, F. K.; Balkenende, A. R.; Verheijen, M. A.; Baklanov, M. R.; Mogilnikov, K. P.; Furukawa, Y. *J. Phys. Chem. B* **2003**, *107* (18), 4280–4289.
(28) Maex, K.; Baklanov, M. R.; Shamiryan, D.; Iacopi, F.; Brongersma, S. H.; Yanovitskaya, Z. S. *J. Appl. Phys.* **2003**, *93* (11), 8793–8841.
(29) Sengupta, S. S.; Park, S. M.; Payne, D. A.; Allen, L. H. *J. Appl. Phys.* **1998**, *83* (4), 2291–2296.
(30) Jeong, T. H.; Kim, M. R.; Seo, H.; Kim, S. J.; Kim, S. Y. *J. Appl. Phys.* **1999**, *86* (2), 774–778.
(31) Choi, S. Y.; Mamak, M.; Speakman, S.; Chopra, N.; Ozin, G. A. *Small* **2005**, *1* (2), 226–232.
(32) Zhang, H. Z.; Banfield, J. F. *Chem. Mater.* **2002**, *14* (10), 4145–4154.

Scheme 1. Standard and Modified Preparation Protocols for the Preparation of Mesoporous and Dense Titania Films

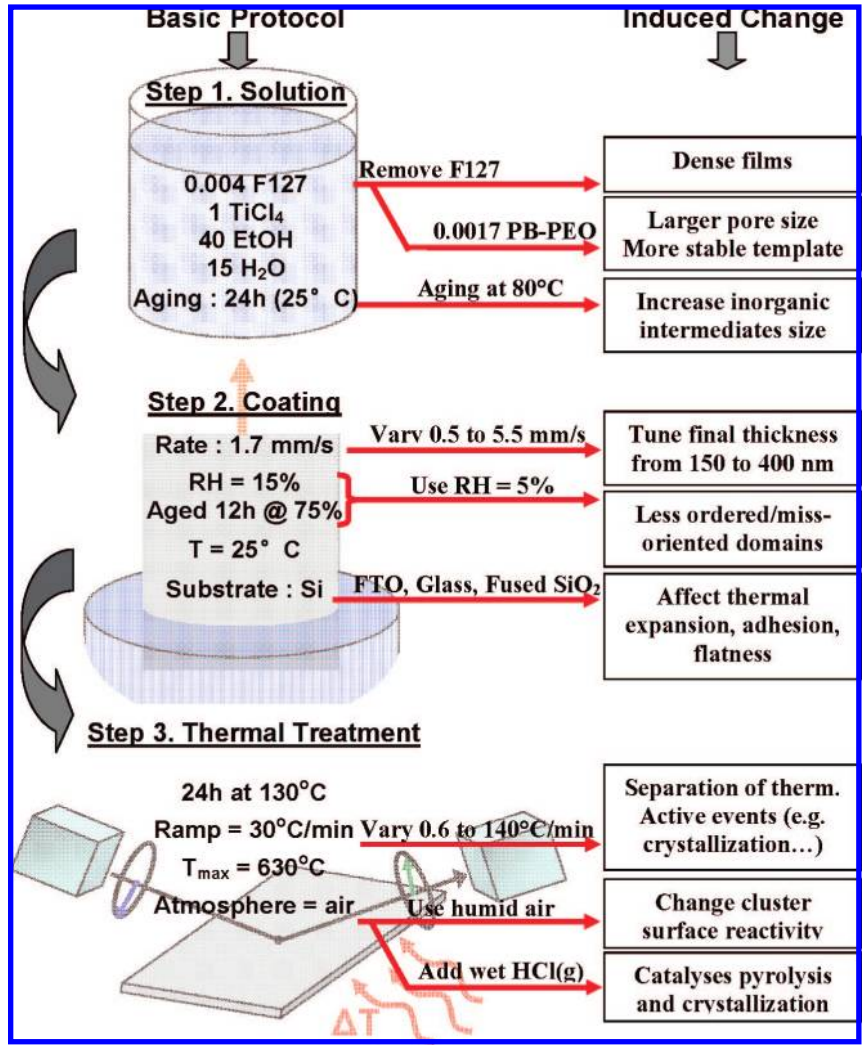

Figures 1 and 2, respectively. Synthesis conditions for templated films were chosen to produce initially cubic *Im3m* films, transitioning to a distorted cubic structure upon thermally driven contraction.[33] These figures display the real component of the composite index of refraction and thickness of the films as a function of temperature as constructed by fitting the ellipsometric data (WASE software) using the optical properties of the silicon substrate at both 65 and 630 °C. The two results were then linearized with respect to the temperature. This method provided excellent accuracy (<0.5% error) for the index of refraction and thickness data for both dense and templated films across all temperature ranges while reducing the computational burden of specifically imputing the optical properties of the substrate for each temperature (Supporting Information).

For both films, the transition from amorphous titania to crystalline anatase is observed at this heating rate starting at ~400 °C, correlating well with HRTEM and in-situ WAXS data reported previously.[14,15] This transition is characterized by a strong increase in the index of refraction and a decrease in the film thickness as the lower refractive index amorphous phase crystallizes into the denser crystalline phase. A continued increase in the anatase fraction is seen until ~500 °C, where the rate of increase in the index of refraction slows. The location of these features is in good agreement with formation of anatase from TEM electron diffraction (Supporting Information) and previous in-situ wide-angle X-ray scattering results.[14]

For dense films, temperatures above 500 °C show the titania matrix continuing to densify, indicated by the decreasing thickness data, while the anatase crystallites grow in size through sintering.[2] In the cooling cycle, the in-situ data show a linear decrease in the index of refraction and the film thickness. The latter corresponds to a volumetric thermal expansion coefficient of $54 \pm 10 \times 10^{-6}$ (K^{-1}, at 20 °C), higher than bulk anatase ($\sim 8-10 \times 10^{-6}$ K^{-1}) but similar to what has been reported for nanocrystalline anatase.[34]

For mesostructured films, the overall ellipsometry behavior is strikingly more complex. This is due to removal of the template and evolution of the porous structure upon anatase crystallization. Increased low-temperature densification is observed for the templated film, attributed to dehydration of the inorganic matrix and rearrangement of the nonionic template affecting the evolution of porosity.[35] After crystallization, the refractive index of the mesoporous film remains outstandingly stable while it increases for the dense films. Such stability must

(33) Crepaldi, E. L.; Soler-Illia, G. J. D. A.; Grosso, D.; Cagnol, F.; Ribot, F.; Sanchez, C. *J. Am. Chem. Soc.* **2003**, *125* (32), 9770–9786.

(34) Jagtap, N.; Bhagwat, M.; Awati, P.; Ramaswamy, V. *Thermochim. Acta* **2005**, *427* (1−2), 37–41.

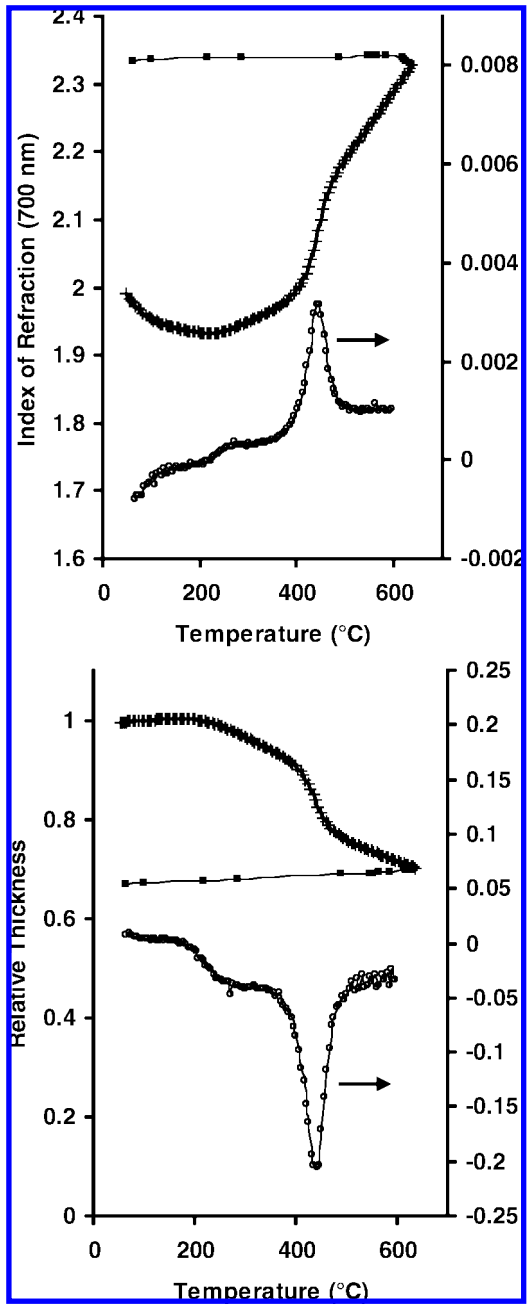

Figure 1. In-situ thermal ellipsometric analysis of a dense titania film at a ramp rate of 30 °C/min. (Top) Index of refraction (at 700 nm) for the (+) heating and (■) cooling cycles and (○) the derivative with respect to temperature during heating (dn/dT, K^{-1}). (Bottom) Relative film thickness during (+) heating and (■) cooling and the derivative with respect to temperature during heating (dh/dT, nm K^{-1}). The initial film thickness was 82 nm.

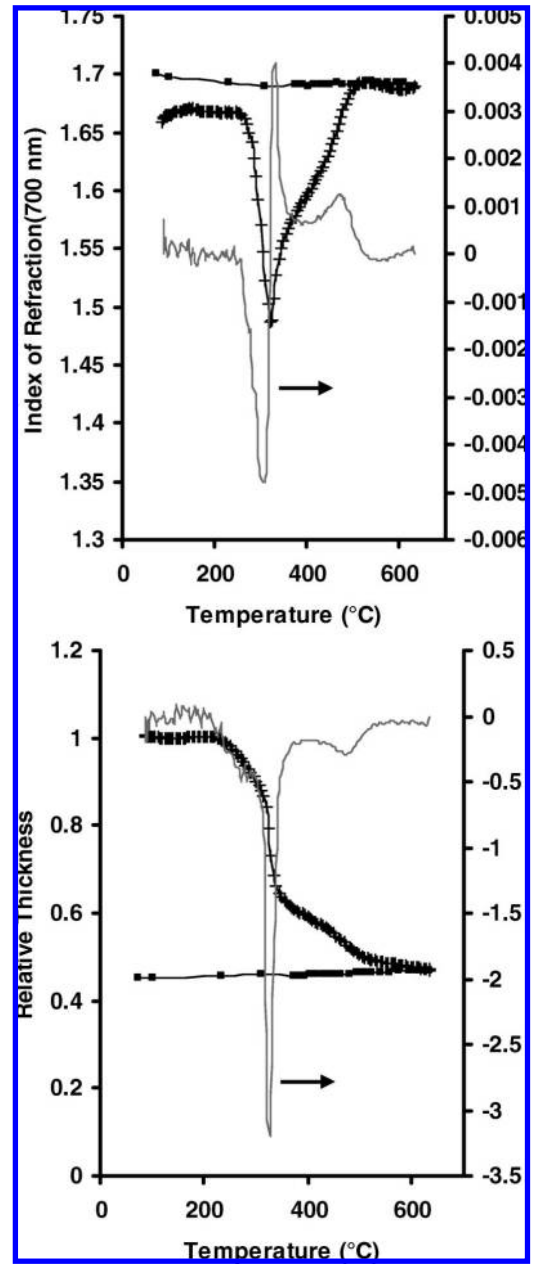

Figure 2. In-situ thermal ellipsometric analysis of a pluronic-templated titania film heated at a ramp rate of 30 °C/min. (Top) Index of refraction for the (+) heating and (■) cooling cycles and (gray) the derivative with respect to temperature during heating (dn/dT, K^{-1}) for the heating cycle. (Bottom) Relative film thickness during (+) heating and (■) cooling and the derivative during heating (dh/dT, nm K^{-1}). The initial film thickness was 262 nm.

be associated to the presence of mesoporosity at high temperature and reduction of sintering. Contraction data obtained via ellipsometry is comparable to in-plane contraction of the mesoporous structure obtained using in-situ SAXS (see ref 14 and Figure 17 below). The cooling cycle gives a value for the volumetric thermal expansion of the film of $70 \pm 10 \times 10^{-6}$ (K^{-1}, at 20 °C). This larger value compared with the dense films suggests that other relaxation processes related to the film structure occur during cooling. The increase upon cooling below ~80 °C is due to water adsorption, and its extent is a function of the pore size and ambient relative humidity (see below). The increase in n on cooling in general correlates to the composite contraction of the film upon cooling.

Template Removal. In-situ thermal ellipsometric analysis can be used to yield detailed information on chemical processes occurring inside mesoporous films. For example, kinetic details on the pyrolysis of the template can be determined. Pyrolysis reactions have been used as model systems for investigating how confinement can effect the rate and selectivity of chemical reactions in mesoprous materials.[36,37]

(35) Galarneau, A.; Cambon, H.; Di Renzo, F.; Fajula, F. *Langmuir* **2001**, *17* (26), 8328–8335.

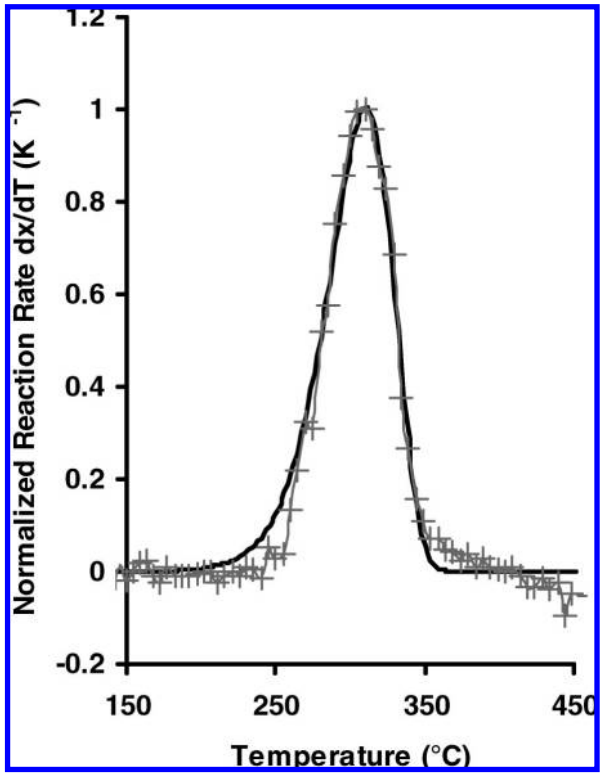

Figure 3. (+) Derivative of the conversion for pyrolysis of the template as a function of temperature compared with (black line) the theoretical normalized reaction rate for a first-order reaction with an activation energy of 121 kJ/mol and a frequency factor of 10^{13} s^{-1}. The heating rate was 30 °C/min.

Comparing the trace of the index of refraction of the F127-templated film (Figure 2) with the dense (Figure 1) film reveals a feature between 250 and 380 °C corresponding to removal of the template. In general, pyrolysis reduces the composite index of refraction while promoting film contraction. Initially, gradual contraction is observed while the index of refraction remains nearly constant due to a compensating creation of porosity by template removal. As the rate of pyrolysis accelerates, increased porosity causes a sharp drop in the index of refraction. Near the maximum rate of pyrolysis (~310 °C) an accelerated decrease in thickness (~30%) occurs as the resulting unstable film structure partially collapses. This sharp decrease in thickness results in a loss of porosity and a rapid increase of the index of refraction as contractional influences exceed the generation of porosity by pyrolysis.

An estimation for the rate of conversion during pyrolysis of the template as a function of temperature is shown in Figure 3. The conversion, x, is estimated from the following relationship, where f_t is the fraction of the film occupied by the template and f_{Vt} is the void fraction in the film created upon pyrolysis

$$x = 1 - \left(\frac{f_t}{f_t + f_{Vt}}\right) \quad (1)$$

These volume fractions are determined through an effective media approximation and by estimating the wall contraction from the contraction of the dense reference film (see Supporting Information). Pyrolysis is again seen to occur between 250 and 380 °C with a maximum rate at ~310 °C. Although pyrolysis is exothermic, it is not expected that the energy released by the small amount of template present in our heating setup would affect these results over the time scales investigated.

Using the method of Redhead, the activation energy for pyrolysis can be estimated using the temperature where the reaction rate reaches a maximum.[38] This analysis gives an activation energy of 124 kcal/mol assuming first-order kinetics with a frequency factor of 10^{13} s^{-1}. First-order kinetics are expected for a reaction in the absence of oxygen diffusion limitations, while the chosen frequency factor is reasonable for a first-order reaction with a small change entropy between the reactant and the transition state; this is expected for an exothermic oxidation reaction (Hammond postulate). These kinetic assumptions can be tested by directly comparing the theoretical conversion as a function of temperature to that calculated from the ellipsometry data, Figure 3. The results show remarkable similarity, supporting the ellipsometric approach for calculating reaction parameters. Small deviations are seen at higher temperatures, >400 °C, as the characteristics of the dense and templated films diverge due to differences in crystallization behavior. This is reasonable considering there is a significantly higher influence of the surface in the porous templated system and that this surface is likely to be polluted by residual carbonated species further inhibiting crystallization. This activation energy using this ellipsometric approach is also in agreement with the value of 131 ± 7 kcal/mol determined previously for pyrolysis of P123 in bulk SBA-15 from thermogravimetric analysis.[39]

Porosity. Templated films show a decrease in the index of refraction between 540 and 630 °C (Figure 2) that is in direct contrast to the increase in the index of refraction for dense films (Figure 1). This discrepancy indicates that the porosity of templated films in this temperature region is increasing. Previous results have shown that the pore structure evolves over this temperature region from a cubic-derived structure to a more open grid-like structure, resulting from pore coalescence due to the densification of titania.[14] Evolution of the porosity of the nanotemplated films can be derived from the in-situ ellipsometry results, Figure 4. The porosity is defined as the void fraction of the film created by pyrolysis of the template plus that created by densification of the matrix parallel to the surface. These fractions are again calculated using an effective media approximation and by estimating the wall contraction from the contraction of the dense reference film (see Supporting Information). The plot is constructed in two parts: the first at low temperatures requiring deconvolution of the influence of the residual template, while after template removal the Bruggeman approximation with a dense film reference is used.

Evolution of porosity is governed by the structural order, the chemical makeup of the matrix and occluded species (water, template, residual carbonaceous species, etc.), and the energy input (heating schedule) that together govern the relaxation pathways. The templated porosity plays a key role in these processes, engendering a large surface energy contribution, large capillary stresses created by high-curvature pores, and by confining the growth of nanocrystals. These factors are espe-

(36) Kidder, M. K.; Britt, P. F.; Zhang, Z. T.; Dai, S.; Hagaman, E. W.; Chaffee, A. L.; Buchanan, A. C. *J. Am. Chem. Soc.* **2005**, *127* (17), 6353–6360.
(37) Kidder, M. K.; Britt, P. F.; Chaffee, A. L.; Buchanan, A. C. *Chem. Commun.* **2007**, 52–54.
(38) Redhead, P. A. *Vacuum* **1962**, *12*, 203–211.
(39) Coutinho, A. C. S. L. S.; Quintella, S. A.; Araujo, A. S.; Barros, J. M. F.; Pedrosa, A. M. G.; Fernandes, V. J.; Souza, M. J. B. *J. Therm. Anal. Calorim.* **2007**, *87* (2), 457–461.

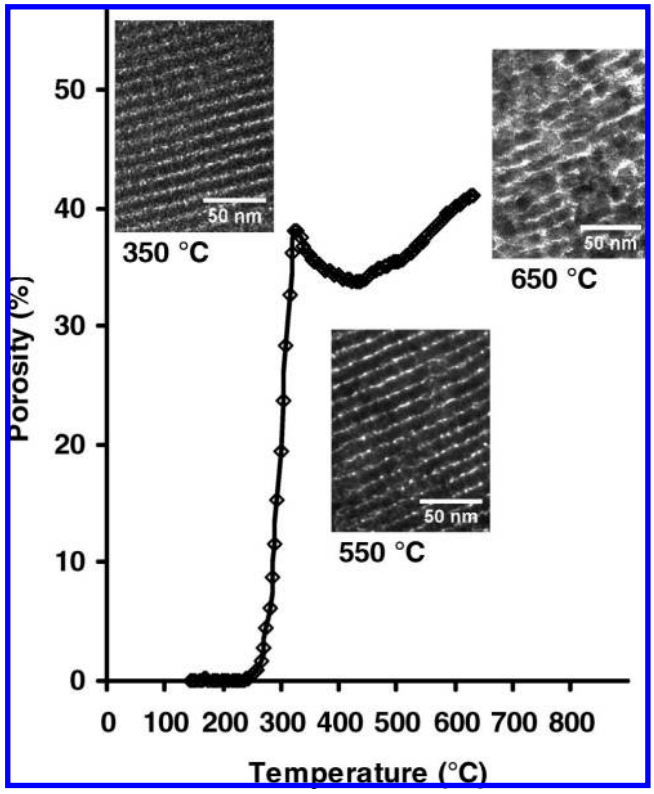

Figure 4. (◇) Porosity as a function of temperature derived from in-situ ellipsometric data. The heating rate was 30 °C/min.

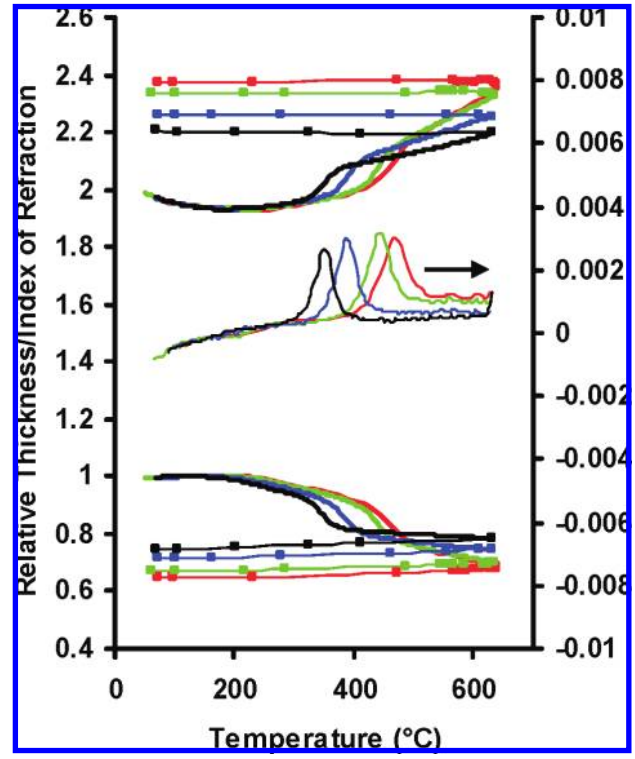

Figure 5. Relative film thickness and index of refraction (at 700 nm) and its derivative with respect to temperature for dense films measured in situ at heating rates of (black lines) 0.6, (blue lines) 2.5, (green lines) 30, and (red lines) 144 °C/min showing the dependence of crystallization on heating rate. Cooling cycle traces are marked by (■).

cially relevant when the surface physically or chemically evolves, such as upon pyrolysis, crystallization, and sintering. Dehydration and pyrolysis of adsorbed species will tend to increase the specific surface energy and thus the capillary pressure. Sintering leads to larger crystallites and adoption of a grid-like pore structure[14] that reduce the energetic contribution associated with curvature.

Figure 4 shows that pyrolysis of the template increases the porosity in the material, reaching a maximum of ∼38% at 330 °C, while there is still some residual template left in the material. At this point film relaxation begins to dominate, resulting in a decrease in porosity that reaches a minimum of ∼34% at 440 °C. This is followed by a region where pore coalescence via sintering dominates. Templated porosity allows densification of the titania to occur in the *XY* directions (wall densification), parallel to the film surface, reducing the thickness of the titania walls and generating porosity. Dense films show a continuous increase in the index of refraction as densification occurs only in the direction normal to the film surface, since the *XY* directions are constrained.[14] It is in response to the above processes and the resolution of internal constraints that the sintering region in particular is seen to take several forms, with the index of refraction increasing, decreasing, or displaying more complex behavior (see below).

Heating Rate. Variation of the heating schedule to control the calcination of oxide materials is one of the most common methods used for optimizing material properties. Such an approach is predicated on balancing several kinetic processes, such as diffusion, condensation, crystallization, and sintering, in order to find material optima among a landscape of metastable (kinetically trapped) phases. Production of titania films balancing accessibility, void fraction, and the type, morphology, and distribution of crystallites for photoactive applications is amenable to such an approach.[2] In-situ thermal ellipsometry of films heated at varying rates are shown for dense and templated films in Figures 5 and 6. In both the dense and mesostructured systems, slow heating rates result in lower crystallization temperatures and less contracted structures with lower indices of refraction. Such reduction of film shrinkage by crystallization has been observed previously in sol−gel titania films at low heating rates, where the crystallites function much like addition of inclusion bodies in mechanically stabilizing the material.[40] A lower crystallization temperature at slower heating rates is expected for a transition characterized by an Arrhenius-type temperature dependence with a positive activation energy.

The apparent activation energy (E_{app}) for the crystallization process can be extracted using an empirical, model-free approach outlined by Pérez-Maqueda et al.[41] using the derivative of the index of refraction data to approximate the extent of reaction, α, from amorphous to crystalline anatase. This extent of reaction considers the crystallization occurring over a temperature range defined by the derivative feature, providing kinetic information on this transition. Kinetically inaccessible titania centers, including initial quantities of pre-existing anatase-like centers and those that remain amorphous even after extensive calcination (thus affecting the final degree of crystallinity), are not considered in this approach. The activation energy is obtained from the slope using a Pearson's linear correlation of reciprocal

(40) Keddie, J. L.; Braun, P. V.; Giannelis, E. P. *J. Am. Ceram. Soc.* **1994**, *77* (6), 1592–1596.
(41) Perez-Maqueda, L. A.; Criado, J. M.; Sanchez-Jimenez, P. E. *J. Phys. Chem. A* **2006**, *110* (45), 12456–12462.

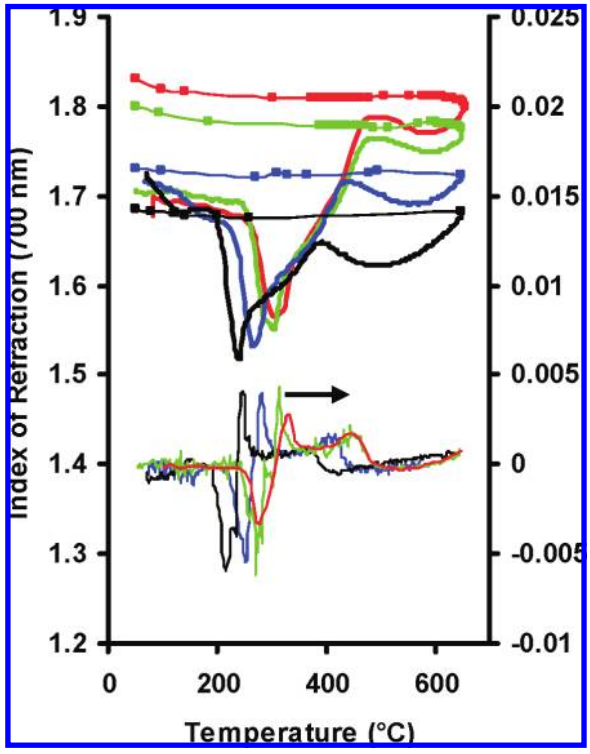

Figure 6. Index of refraction and its derivative with respect to temperature for mesoporous films measured in situ at heating rates of (black lines) 0.7, (blue lines) 2.5, (green lines) 30, and (red lines) 100 °C/min showing the dependence of crystallization on heating rate. Cooling cycle traces are marked by (■).

temperature and the integral form of the simplified Sestak−Berggren[42] kinetic equation.[41]

For dense films this analysis, fitted over four different heating rates (spanning 2 orders of magnitude) and taking α from 0.05 to 0.75, gives an observed activation energy of 150 kJ/mol. The same observed activation energy is extracted fitting to a Johnson, Mehl, and Avrami (JMA) crystal growth model using the same approach.[43–47] The JMA *n* value, a parameter encompassing the nucleation and growth mechanisms and the dimensionality, from this analysis is 1.5 (see Supporting Information). For templated films, the observed activation energy for crystallization is 185 kJ/mol using both the empirical and the JMA model, while the JMA model yields a value for *n* of 0.85. Nearly identical values were obtained[48] ($E_{app} = 210 \pm 40$ kJ/mol and $n = 0.9 \pm 0.1$) via in-situ XRD analysis of cubic titania films templated with P-123 (a slightly larger apparent activation energy would be consistent with the fact that P-123 is a smaller template than F127, producing smaller pores and thus magnifying the templating effect, see below).

For both films, the kinetics displayed are broadly consistent across the heating ranges investigated, indicating a common mechanism regardless of heating rate. Furthermore, these crystallization mechanisms follow Arrhenius kinetics up to conversions of 0.75, after which nonlinearities, possibly caused by the impingement of growing particles, are observed.

The values for the JMA parameter can be used to help classify the processes that may be involved in crystallization. In general, this parameter is lower for systems with preformed nucleation centers, low-dimensional growth mechanisms, and growth limited by diffusion to the crystal−amorphous phase interface as opposed to through this interface.[43] We postulate that the *n* value of 1.5 for dense films originates from 3D diffusion-controlled growth from preformed nucleation centers in the bulk. Such centers are likely anatase-like titania nanoclusters, which have been observed previously at low temperatures by XANES.[49] Other kinetic processes consistent with an *n* of 1.5, including low-dimensional (between 1D and 2D) growth limited by diffusion through the phase boundary of growing crystallites or 1D diffusion-controlled growth from continuously nucleating surfaced regions, are less satisfying as they rely on mechanisms promoted by surface effects. Such surface promotion is not supported by the increased difficulty in crystallizing materials with high surface areas and lack of a kinetic dependence on the thickness of dense films (see below).

Mesostructured films, with an *n* value between 0.5 and 1, can be ascribed to low-dimensional (1−2D) diffusion-controlled growth from preformed nucleation centers. The differentiation between pre-existing bulk and surface centers is immaterial since the ubiquitous surface would not constrain, dimensionally, bulk crystallization nucleated from the surface. Equivalent 1D diffusion-controlled growth has been proposed for 2D hexagonal periodic mesoporous thin films.[31] The existence of preformed nucleation centers in the matrix is again consistent with discrete anatase-like clusters formed under the applied chemical conditions[15,33,49] and is seen in the electron diffraction correlation distances at 300 and 350 °C (Supporting Information).

Given the kinetic mechanisms above, the larger E_{app} for templated materials may derive from the ability of the surface to disrupt transport-driven processes, such as diffusion of material to the crystal−amorphous phase interface. Dimensional effects, structuration of the interface, or the influence of residual impurities are likely factors in this. Some degree of surface structuration is expected due to the geometrical requirements at the surface in terms of bonding, etc., as compared to the bulk. Residual carbonaceous species originating from incomplete pyrolysis, known to exist under certain conditions for mesoporous SiO_2−Pluronic systems,[50] may also be an influence given both the larger surface area and the larger initial organic content in templated films. Restricted transport at the surface due to any of these processes would destabilize crystallization in the high surface area templated system. Delayed crystallization in the templated system may also result from a change in the distribution of anatase-like clusters. At the interface, the number of these clusters and/or their ability to support crystal growth (i.e., to serve as nucleation centers) is not expected to follow that of bulk species due to interfacial constraints including absorption and surface restructuration.

Calcination Environment. Absorbed water is a critical component in the thermodynamics governing the stability of nanosized titania.[17] As such, it can be expected that the presence or absence of water during calcination would affect the resulting

(42) Sestak, J.; Berggren, G. *Thermochim. Acta* **1971**, *3*, 1.
(43) Perez-Maqueda, L. A.; Criado, J. M.; Malek, J. *J. Non-Cryst. Solids* **2003**, *320* (1−3), 84–91.
(44) Avrami, M. *J. Chem. Phys.* **1939**, *7* (12), 1103–1112.
(45) Avrami, M. *J. Chem. Phys.* **1940**, *8* (2), 212–224.
(46) Avrami, M. *J. Chem. Phys.* **1941**, *9* (2), 177–184.
(47) Johnson, W. *Trans. Am. Inst. Min. Metallurg. Eng.* **1939**, *135*, 416.
(48) Kirsch, B. L.; Richman, E. K.; Riley, A. E.; Tolbert, S. H. *J. Phys. Chem. B* **2004**, *108* (34), 12698–12706.
(49) Angelome, P. C.; Andrini, L.; Calvo, M. E.; Requejo, F. G.; Bilmes, S. A.; Soler-Illia, G. J. A. A. *J. Phys. Chem. C* **2007**, *111* (29), 10886–10893.
(50) Kleitz, F.; Schmidt, W.; Schuth, F. *Microporous Mesoporous Mater.* **2003**, *65* (1), 1–29.

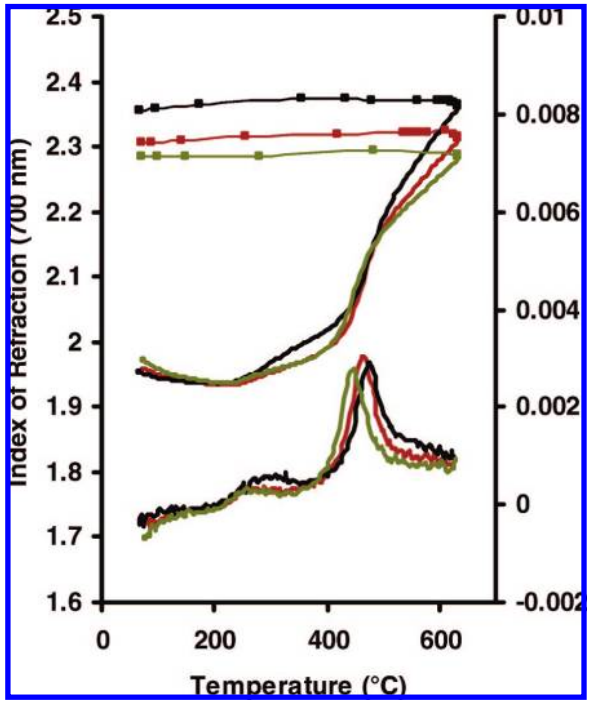

Figure 7. Index of refraction (at 700 nm) and its derivative with respect to temperature measured in situ for dense films under a water vapor pressure of (green line) 3.0 and (red line) 1.2 kPa as well as under (black line) argon. This corresponds to a water density in the feed (at 25 °C) of 22, 9, and 0 g m^{-3}, respectively. Cooling cycle traces are marked by a solid box (■).

nanomorphology by influencing, for example, the energetics of intermediate nanostructures. Figures 7 and 8 show that the presence of water during calcination has a profound effect on the evolution of the titania structure for both dense and templated films. For dense films, changing the partial pressure of water in the incoming feed (25 °C) from 0 to 3.0 kPa (~3 vol % or 100% RH at 25 °C) reduces the final index of refraction from 2.36 to 2.28 and causes a 30 °C shift in the position of the crystallization feature from 477 to 447 °C.

For templated films, changing the partial pressure of water in the incoming feed (25 °C) from 0 to 13 kPa (~13 vol % or 100% RH at 50 °C) lowers the final index of refraction from 1.77 to 1.62. Using the Bruggeman approximation and taking into account the corresponding changes in the dense films, this corresponds to an increase in the final void fraction from 0.31 to 0.42. This is remarkable in that the water content of the incoming stream is relatively low with as little as 1 vol % increasing the porosity by 10%. The temperature of crystallization is also significantly affected by the presence of water, with a shift in $(dn/dT)_{max}$ associated with crystallization by 45 °C, from ~440 °C at a partial pressure of 13 kPa to ~480 °C in a dry atmosphere.

To test if these effects are due to chemistry occurring at low temperatures, where water adsorption is known to lead to chemical changes in the network through condensation,[51] we looked at the effect of adding water above 300 °C, Figure 9. At these temperatures water would not be expected to exist as a condensed phase, even in highly confined environments. Switching at 300 °C from dry conditions to just 3 vol % water results in near identical affects to those seen above, decreasing

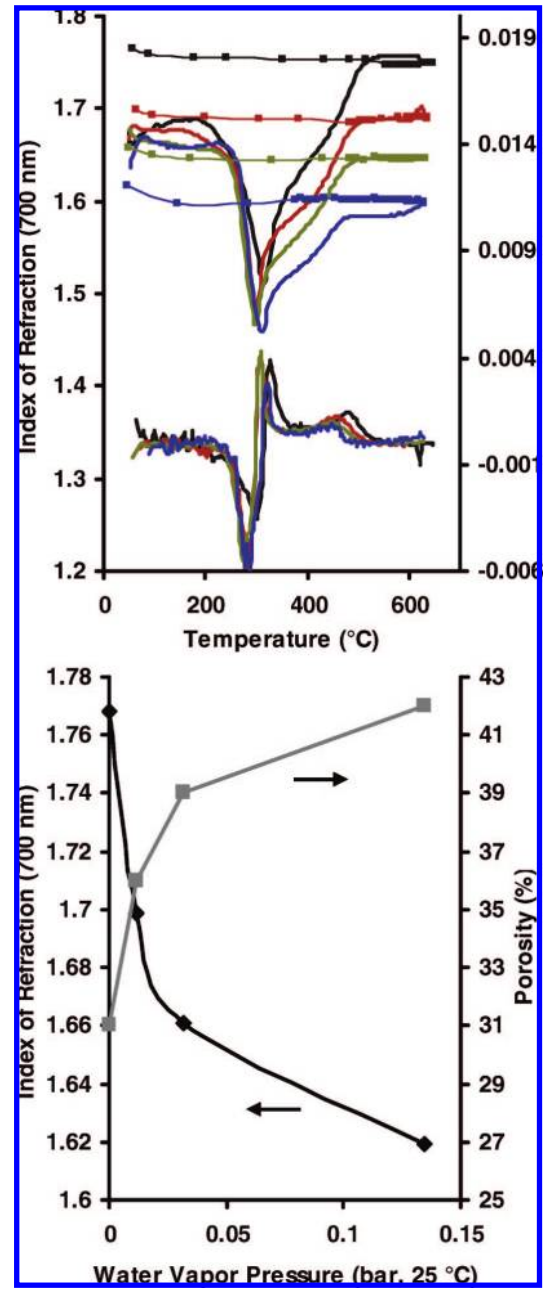

Figure 8. (Top) Index of refraction (at 700 nm) and its derivative with respect to temperature measured in situ for dense films under a water vapor pressure (at 25 °C) of (blue line) 13.7, (green line) 3.2, and (red line) 1.2 kPa as well as under (black line) argon. This corresponds to a water density in the feed (at 25 °C) of 100, 23, 8, and 0 g m^{-3}, respectively. Cooling cycle traces are marked by a solid box (■). (Bottom) Final index of refraction and porosity as a function of water in the calcination atmosphere.

the index of refraction by ~0.1 and the crystallization temperature by ~15 °C. This indicates that the effect of water is most pronounced above 300 °C in the high-temperature environment after removal of the template.

For some insight into the nature of such water absorption at these high temperatures, we exposed a templated film previously calcined under argon to 415 °C to 3 vol % water vapor at 300 °C and observed the results using in-situ ellipsometry, Figure 10. The 415 °C calcination temperature was chosen in order to achieve template removal and stabilization of the oxide network without causing significant crystallization. This can be seen in

(51) Burgos, M.; Langlet, M. *J. Sol-Gel Sci. Technol.* **1999**, *16* (3), 267–276.

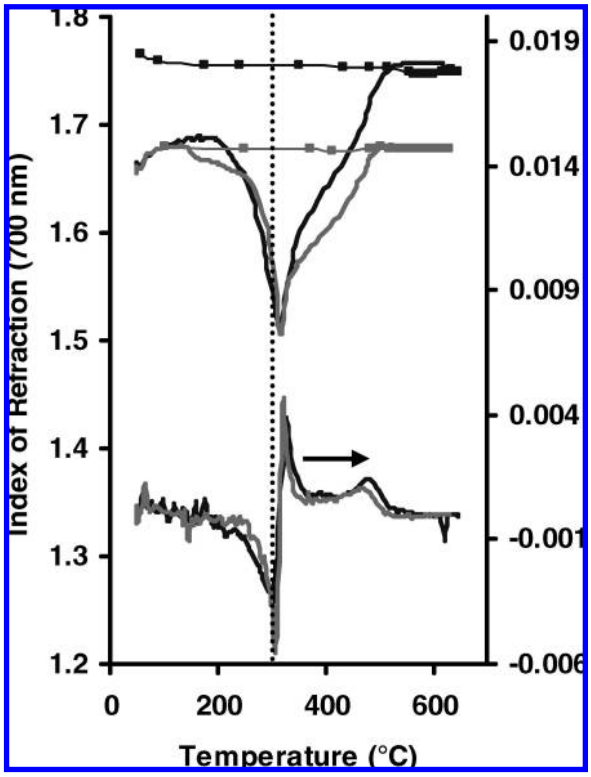

Figure 9. In-situ thermal ellipsometric analysis showing the index of refraction and its derivative with respect to temperature of a pluronic-templated titania film heated at a ramp rate of 30 °C/min for (black line) a sample calcined under argon and (gray line) a sample calcined under argon up to 300 °C and then under a water vapor pressure of 3.2 kPa (at 25 °C, or ∼3 vol %). The switch for this latter material is marked by the vertical dotted line. Cooling cycle traces are shown by a solid box (■).

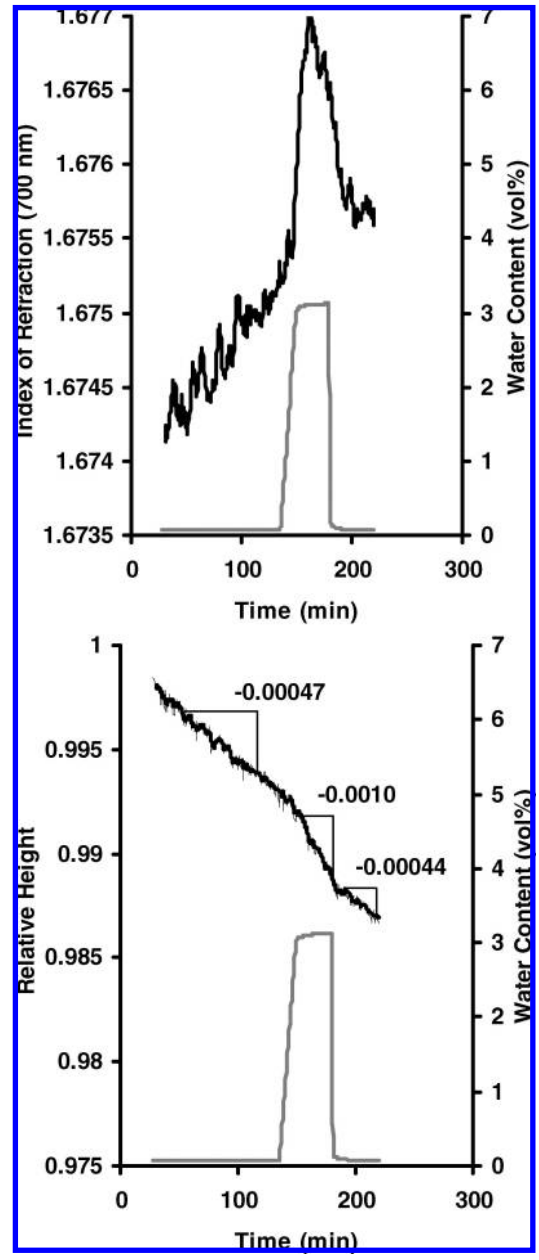

Figure 10. In-situ thermal ellipsometric analysis of a pluronic-templated titania film initially calcined to 415 °C upon exposure to water at 300 °C. (Top) Index of refraction and (bottom) the relative thickness heated both show changes in the presence of a wet atmosphere. For clarity, the index of refraction data have been smoothed using a fourth nearest-neighbor averaging.

Figure 9, where, at this heating rate under argon, heating to 415 °C lies in the plateau situated between the template pyrolysis feature and the crystallization feature. Upon cooling to 300 °C in a dry atmosphere, the film index of refraction is seen to increase while the thickness decreases, indicating that the film continues to undergo, albeit slowly, relaxation processes at this temperature. The processes, however, are small and nearly linear over the time periods studied. Addition of 3 vol % water into the feed stream results in an apparent reversible increase in the index of refraction and an acceleration, by a factor of ∼2, of the rate of irreversible contraction. The increase in index of refraction corresponds, using the Bruggeman approximation, to ∼0.1 vol % water adsorption. This is a very rough estimate since the nature of the adsorption and hence its ultimate effect on the composite index of refraction is not known. The data suggest that at least part of this water adsorption is reversible due to the reduction of the index of refraction upon returning to a dry environment. Given the additional contraction in thickness, however, the final index is lower than would be expected, suggesting that there is an irreversible chemical change to the nature of the framework.

The effect of water on the final index of refraction in the materials can be ascribed to several processes. Analogous to lowering the heating rate, the lower final index of refraction in the presence of water is likely partially due to the earlier onset of crystallization in these systems. Promotion of crystallization in the presence of water has been seen in low-temperature vapor studies (250 °C) and is utilized in hydrothermal treatments.[18,19,52,53] Water is postulated to promote anatase nucleation by rearrangement of the amorphous structure through surface adsorption.[18,53] An increase in the number of pre-existing nucleation sites would effectively increase the rate of crystallization and result in smaller crystallite sizes. Such smaller crystallite sizes have been observed previously comparing dense, sol−gel-derived films calcined in argon or low vacuum compared to air calcined

(52) Imai, H.; Morimoto, H.; Tominaga, A.; Hirashima, H. *J. Sol-Gel Sci. Technol.* **1997**, *10* (1), 45–54.
(53) Yanagisawa, K.; Yamamoto, Y.; Feng, Q.; Yamasaki, N. *J. Mater. Res.* **1998**, *13* (4), 825–829.

films.[54,55] Similarly, an increase in the index of refraction has been observed for films calcined in argon or low vacuum.[55,56]

A significant part of the effects of water on producing lower index of refraction materials originates between 300 °C and the onset of crystallization. The absorption experiment at 300 °C shows that water can reversibly incorporate into the system, but the presence of water causes irreversible contraction of the film thickness that is not accompanied by a significant irreversible increase in index of refraction. This is an indication of an irreversible change in the internal structure of the material upon water exposure. Contraction of the material that is not accompanied by an increase in the index of refraction could result from a net reduction in the number of polarizable particles per unit volume through condensation processes. Such condensation would tend to stiffen the material and increase the matrix viscosity, much like with crystallization discussed above.[40] This reduces the long-term potential for shrinkage by choking off diffusive-type sintering and structural relaxation processes that are responsible for a large portion of contraction in sol−gel-derived materials.[57] This would especially be the case if water was facilitating the earlier creation of more stable, anatase-like oligomeric structures as proposed previously.[18,53]

At moderate temperatures (<250 °C), the presence of chloride has been suggested to facilitate rearrangement of the titania nanobuilding blocks constituting the matrix walls into ordered structures, which can resemble local crystalline order.[49] This effect has been explored by XANES in low-temperature-treated titania samples that are classified as amorphous by routine XRD.[49] A complementary analysis of the structural effect promoted by chloride on the development of film morphology was explored by adding wet HCl to the incoming feed, Figure 11. This causes an initial increase in the index of refraction at low temperatures, presumably due to adsorption and densification. The temperature of pyrolysis reduces by ~60 °C due to the oxidizing nature of HCl with a maximum rate centered at ~215 °C. More dramatically, the stability of the resulting matrix is considerably higher with contraction greatly arrested upon pyrolysis. This trend remains even during calcination and sintering, resulting in a final material with an index of refraction of ~1.45 and ~55% porous volume.

Effect of Solution Aging. Aging of the dipping media is known to affect materials prepared by EISA due to the chemical evolution of inorganic species, from monomers to oligomeric clusters and nanoparticles. The degree of condensation in solution of these inorganic entities changes both the ability to self-organize with the surfactant−template interface and the kinetics of further condensation during material post-treatment.[11,12] Here, no significant differences are seen in the film thickness due to aging effects. Such an effect would likely evolve from extended conjugation increasing the solution viscosity. However, unlike in silica systems, the precursors used here tend to remain as oligomeric clusters in solution that have little effect on the solution viscosity, even after extensive aging.[33] Solutions aged at 80 °C for even short periods of time (<1 h), however, resulted in noticeable changes in the thermal behavior in both dense and templated films, Figure 12. Aging in dense films led to a slight increase in the crystallization temperature from ~445 to 460 °C but a decrease in the index of refractions of the matrix wall. This behavior is opposite to that seen above for variations in the heating rate and water content where higher crystallization temperatures lead to denser materials with larger indices of refraction. A significant fraction of this lowering of the index of refraction with aging is present at low temperatures (after curing overnight at 130 °C), while the rest of the effect emerges during crystallization. This is consistent with formation of larger inorganic clusters, allowing greater interstitial microporosity upon packing in the matrix wall and greater stability toward incorporation into growing crystallites resulting in higher crystallization temperatures. These structures can retard shrinkage by increasing the viscosity of the matrix, as discussed above upon addition of water to the calcination environment. For templated films, less obvious changes were noticeable in the crystallization temperature and the initial index of refraction after curing. Moreover, only the more highly aged solutions caused significant effects. This suggests perhaps that structurization at the interface, which dominates the matrix behavior, is already serving a similar role by having an effective scale that is correspondent with oligomers created through aging for short periods of time at 80 °C. Only at higher aging time (~1 h) are the crystallites large enough to affect the material behavior. The Bruggeman approximating based on the index of refraction of the dense films reveals that there is little change to the resulting mesoporosity in the templated materials and that the differences due to aging is mainly confined to the matrix walls.

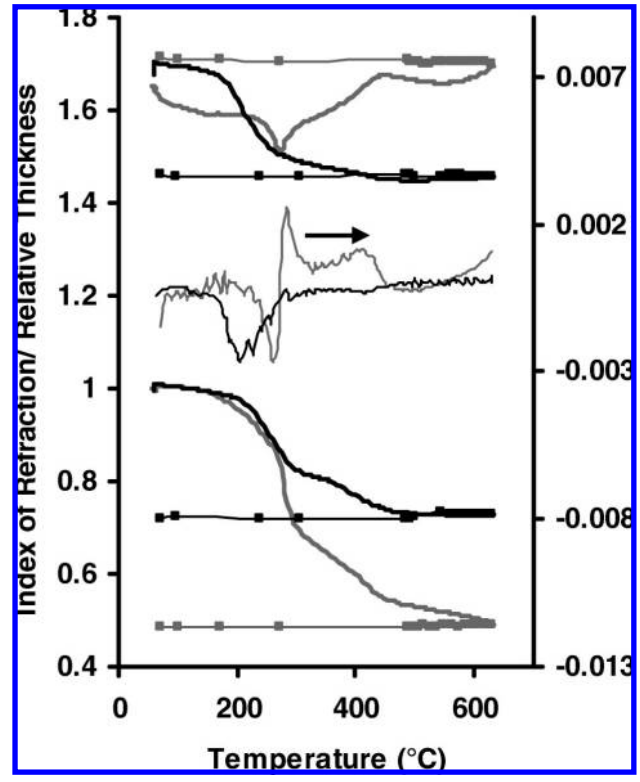

Figure 11. Relative film thickness and index of refraction and its derivative with respect to temperature measured in situ for mesoporous films heated at 30 °C/min under a water vapor pressure (at 25 °C) of 3.2 kPa in the (black line) presence and (gray line) absence of HCl vapor. Cooling cycle traces are marked by solid box (■). Films were initially 307 nm thick.

Film Thickness/Substrate Effects. The influence of the substrate is potentially an important factor in the design and control of thin films since this influence, which can fully or

(54) San Vicente, S.; Morales, A.; Gutierrez, M. T. *Thin Solid Films* **2002**, *403*, 335–338.
(55) Sreemany, M.; Sen, S. *Mater. Res. Bull.* **2007**, *42* (1), 177–189.
(56) Yoldas, B. E. *Appl. Opt.* **1982**, *21* (16), 2960–2964.
(57) Brinker, C. J.; Scherer, G. W.; Roth, E. P. *J. Non-Cryst. Solids* **1985**, *72*, 345–368.

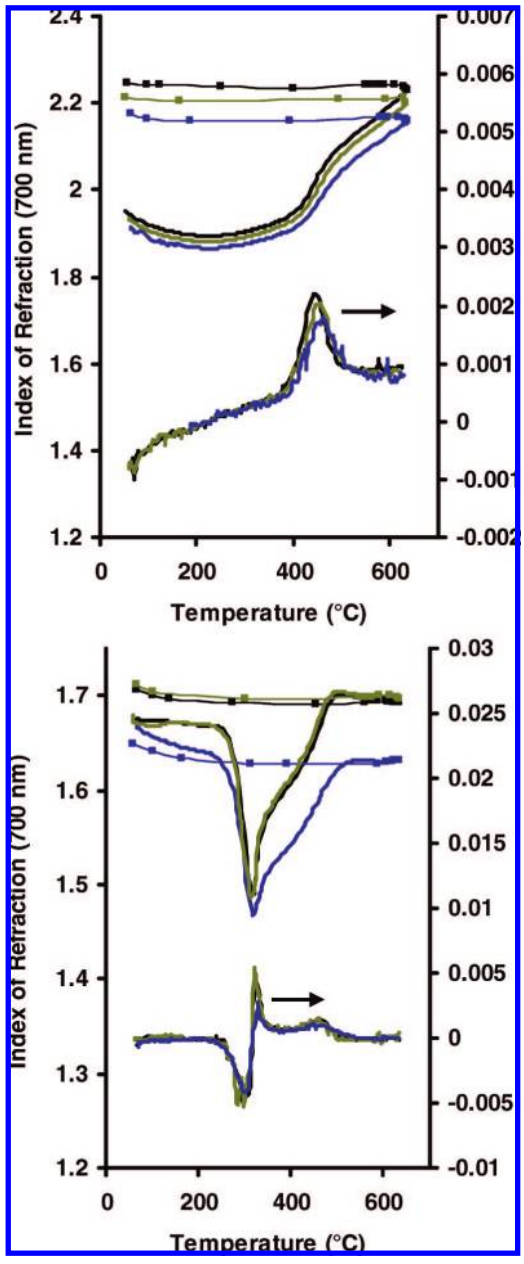

Figure 12. Index of refraction (at 700 nm) and its derivative measured in situ for (top) dense and (bottom) templated films made with (black line) fresh solutions and solution that had been aged for (green line) 20 and (blue line) 80 min at 80 °C. Cooling cycle traces are marked by a solid box (■).

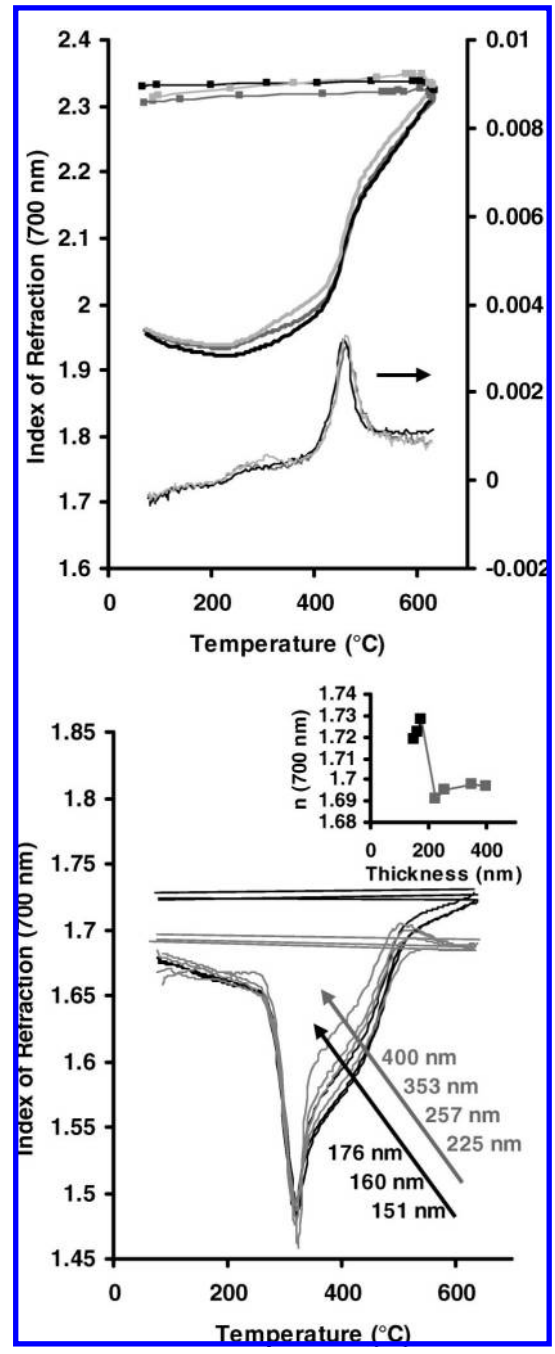

Figure 13. Index of refraction (at 700 nm) and its derivative with respect to temperature measured in situ for films of various thicknesses on silicon wafers: (top) dense films with thicknesses (at 120 °C) of (black line) 119, (dark gray line) 63, and (light gray line) 51 nm (final thicknesses were 79, 42, and 34 nm, respectively, cooling cycle traces are marked by a solid box (■)), and (bottom) templated films with initial thicknesses (dry at 120 °C) (black lines) between 150 and 176 nm and (gray lines) between 225 and 400 nm. The order of these series is indicated by the arrows, with thinner films delaying crystallization. (Inset) Final value of the index of refraction (measured ~100 °C) as a function of temperature shows a jump in behavior between 175 and 225 nm. For clarity, cooling cycle traces are shown as a linear regression. All films were heated at 30 °C/min at 38% RH.

gradationally extend across the thickness of the film, can be used to modify the film properties. Ordering and crystallization effects, for example, have been observed in mesostructured silica and titania films.[49,58,59] Two methods were used to evaluate these processes. The first, Figure 13, evaluates the film behavior as a function of the film thickness. Thinner films should be more sensitive to the presence of the substrate as these films will be, on average, more susceptible to material diffusion, adhesion, and epitaxial effects. Moreover, film thickness is a critical parameter in the design of photoactive and optical devices, and variations in film properties with thickness have important repercussions in this regard.[21,22] Figure 13 shows the in-situ development of dense and templated films as a function of thickness. For dense films, the in-situ behavior is nearly independent of thickness over this range with no apparent net effect on the final index of refraction or the crystallization

(58) Chougnet, A.; Heitz, C.; Sondergard, E.; Berquier, J. M.; Albouy, P. A.; Klotz, M. *J. Mater. Chem.* **2005**, *15* (32), 3340–3345.
(59) Zhang, Y.; Li, J.; Wang, J. *Chem. Mater.* **2006**, *18* (12), 2917–2923.

temperature. That the crystallization temperature remains unchanged suggests that the alternative kinetic model, 1D diffusion-limited growth from nucleation sites originating from the interface (see above), is unlikely.

For templated films, there is a marked step change in the final index of refraction between 175 and 225 nm, Figure 13 (inset). Above this threshold films show decreasing indices of refraction in the sintering regime (>450 °C) resulting in final index of refraction values of less than 1.7. In contrast, films below this threshold show increasing indices of refraction in this regime (much like dense films) and give final index of refraction values between 1.72 and 1.73. In both series, thicker films show increasing index of refraction values upon template removal, indicating a larger relaxation of the matrix for thicker films. No significant change was seen in the crystallization temperature, and all films appeared crack free by both optical microscopy and AFM.

Evolution of the refractive index during sintering and after pyrolysis as a function of thickness points to an influence of the substrate on film shrinkage. The two behaviors indicate a reduction in the ability of the film to undergo relaxation as the film thickness is reduced. This is likely due to adhesive constraints imposed on the film by the substrate. That this constraint is limited to templated films stresses the importance of surface-related and/or dimensional effects on the relaxation processes in these mesostructured materials.

Adherence to the surface and the resulting constraints on the matrix should influence the final morphology of the material, making these results interesting from a device prospective, such as applications as photocatalysts. Moreover, in a broader context, the film sensitivity to the substrate places a minimum bound on thickness that must be achieved in order to transfer ellipsometric results (that can only be obtained for film geometry) to other geometries such as fibers, particles, etc.

A second route to gauge the influence of the substrate, Figure 14, is to observe the evolution of films deposited on different substrates. For dense films the final index of refraction follows the order glass < FTO (fluorine-doped SnO_2, ~100 nm, supported on glass) < silicon < fused silica. A higher index of refraction value for dense films on quartz compared with glass has been reported previously and ascribed to ion diffusion from glass into titania films.[56] Specifically, Auger spectroscopy showed the presence of Na ions concentrated on the surface of the film at temperatures above 400 °C and Ca ions distributed uniformly in the film at temperatures above 450 °C.[56] Significant differences are also seen in terms of the crystallization temperature, being lowest on the silicon substrate and increasing for FTO and fused silica. Glass shows the highest crystallization temperature, resulting from the presence of diffused ions. The profile of this feature is also significantly broader, indicating a different crystallization mechanism on this substrate in the presence of these diffused ions. The fused silica substrate is unique in that it shows radically different behavior at low temperatures in a regime where structural changes are often dominated by capillary contraction and condensation processes.[40,57] The higher index of refraction at these low temperatures on fused silica is not accompanied by significant deviations in the film thickness, which remains roughly constant below 250 °C, as in Figure 1 for the silicon substrate. It is assumed that the behavior on fused silica is a consequence of its low coefficient of expansion, although the specific mechanism warrants further investigation.

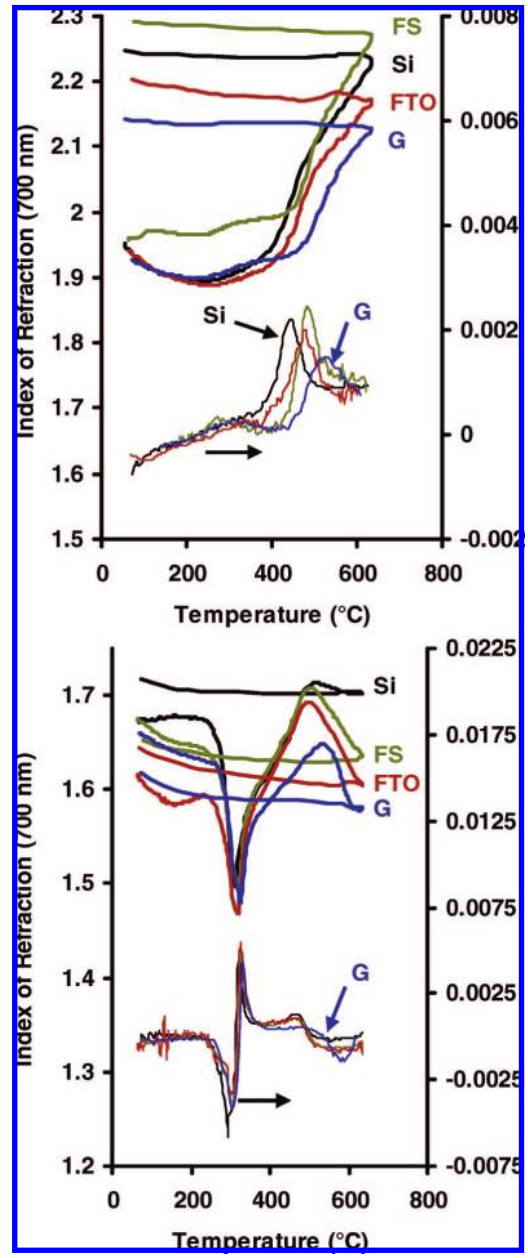

Figure 14. Index of refraction (at 700 nm) and its derivative with respect to temperature measured in situ for (top) dense and (bottom) templated films on (black line) silicon wafers (Si), (green line) fused silica (FS), (red line) fluorine-doped tin oxide (~100 nm) supported on glass (FTO), and (blue line) glass (G).

The change in crystallization temperatures for the various substrates, being lowest for the silicon substrate, is believed to be a consequence of adhesive constraints imposed on the film by the substrate. As above when varying the film thickness, these constraints affect the ability for the film to undergo relaxation, thus impacting the structure within the film and the initial material state from which crystallization occurs.

With the exception of the glass substrate, the templated films show virtually no substrate dependence on the crystallization temperature. The difference in the two systems being crystallization in the templated system is dominated by surface effects (dimensionality, structuration, residual carbonaceous species, etc.). As in the dense system, a higher crystallization temperature is observed on the glass substrate, which may be explained by ion diffusion into the film. Suppressed crystallization has been

seen previously in mesoporous titania films supported on glass substrates, resulting in diminished photocatalytic behavior.[49,59] No significant substrate effect is seen in the position of the pyrolysis feature, while strong effects are seen upon curing at low temperatures and during sintering. At low temperatures, structural changes are often dominated by capillary contraction and condensation processes,[40,57] so differences could be expected based on film−substrate adhesion and interfacial energy. After crystallization, silicon films seem to be unique in that the index of refraction remains relatively unperturbed, while on the other substrates large decreases are seen due to the generation of porosity during sintering. This sintering results in materials with significantly lower final indices of refraction and a loss of mesostructural order. The lack of sintering in the silicon system is believed to be due to its relative rigidity as a monocrystalline support to support high adhesion with the titania coating and, perhaps, by extension of the dense system its ability to promote crystallization near the surface. These two processes should restrict the movement of material required for viscous sintering. The other substrates show increasing sintering based on the expected pliability of the materials with the glass and ITO crystallites supported on glass being the most prone to sintering. The fused silica substrate may be softer than otherwise expected due to the possibility of titania ions diffusing into the surface layer.[60] Moreover, due to the flatness of the silicon substrate, the mesostructured film may be better aligned and therefore more structurally robust. In general, the nature of the substrate results in changes to the evolution of the templated film that is relatively large compared to variations with film thickness, an important consideration in material design.

Effect of Ordering. The mesoscale organization of thin films is of great interest in terms of how such organization can be used to increase the surface area, facilitate access to active sites, perturb physical and chemical processes through confinement effects, and so on. For example, organizational effects have recently been investigated in the context of photocatalysis for titania films having 3D cubic mesostructure compared to transversally aligned 2D hexagonal mesostructure.[23] Here we compare the structural evolution during thermal treatment of ordered *Im*3*m* cubic films to less-ordered films. The latter prepared with the same starting solution but under low relative humidity dip-coating conditions.[11] The difference in ordering is characterized by a loss of the preferential orientation of the ordered domains (diffraction ellipse) and a slight deviation of the porous network corresponding *d* spacing (slightly more diffuse signal) for the less-ordered film (see Figure 15). While there is virtually no difference between the two materials prior to template removal, in-situ ellipsometry, Figure 15, reveals significant deviations just after removal of the template. The less ordered structure shows a much larger relaxation event after template removal with a large increase in the index of refraction. This is followed by a significantly larger decrease in the index of refraction after crystallization due to sintering. The crystallization profile is also perturbed with a sharper crystallization feature for the less ordered structure that is more reminiscent of dense films. Ex-situ GISAXS investigation (Elettra synchrotron SAXS line in Trieste, Italy) reveals the different degree of ordering for the two films at 400 °C and the slightly larger (14 versus 13.1 nm in the [1−10] direction), more narrowly distributed periodicity for the ordered film. The ordered film also shows a more well-defined cubic-derived structure after

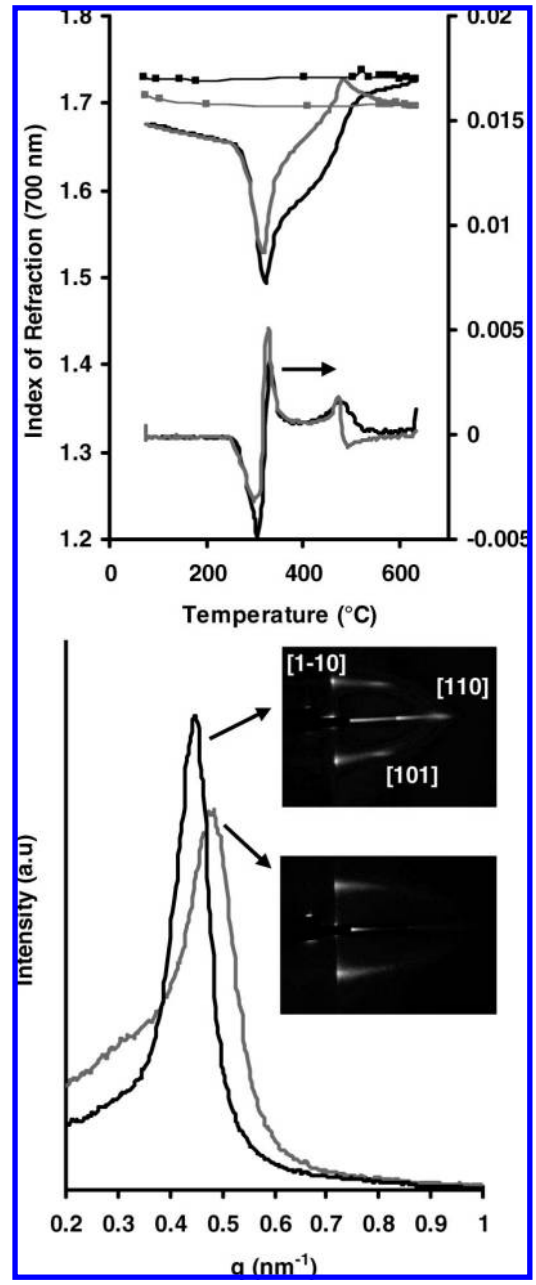

Figure 15. (Top) Index of refraction and its derivative with respect to temperature measured in situ (black line) on ordered pluronic film and (gray line) and a film synthesized under conditions leading to a disordered film. Initial film thicknesses were 177 and 207 nm, respectively. Cooling cycle traces are marked by a solid box (■). (Bottom) Intensity of GISAXS signal in the [1−10] direction for the (black line) ordered and (gray line) poorly ordered film calcined to 400 °C.

stabilization at 130 °C, while after calcination to 630 °C peaks remain sharper (data not shown). Water adsorption−desorption using environmental ellipsometry porosimetry (EEP) of films calcined to 630 °C, Figure 16, show that the two materials have broadly similar accessible pore volumes with the well-ordered material having slightly smaller, more narrow pore size distributions for the adsorption and desorption branches (inset). The sorption data also show the less-ordered film to be slightly unstable to the process of filling and emptying with water, with the desorption branch of the isotherm not returning to the same index of refraction value at the completion of the cycle. This, along with the greater relaxation of the structure after template

(60) Rose, A.; Exarhos, G. J. *Thin Solid Films* **1997**, *308*, 42–49.

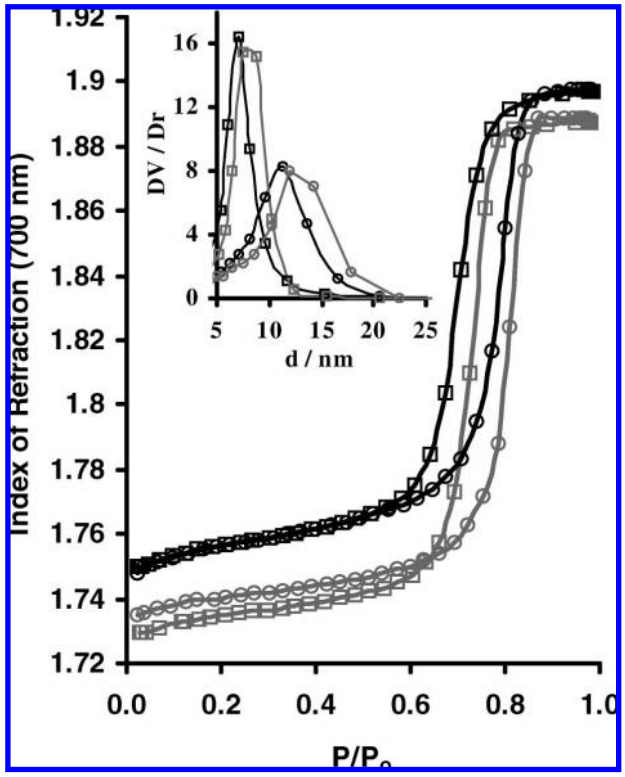

Figure 16. Water (○) adsorption and (□) desorption isotherms for (black line) well-ordered and (gray line) less ordered films calcined to 630 °C. (Inset) Pore size distributions determined using EEP with the adsorption branch showing the pore size distribution of the large axis parallel to the film surface and the desorption branch showing the size of pore interconnections.

removal, suggests that ordering provides a much more resilient matrix scaffold given a similar pore size distribution. The differences in sintering behavior also suggest that an ordered structure can more effectively maintain the stability of the network, reducing material displacement by providing a more internally balanced structure through a higher degree of mesoorder symmetry in the direction normal to the surface. The integrity and balance of the interface is apparently also not sufficient to provide a check on crystal growth in the less ordered films since the sharper crystallization peak suggests that the more collapsed porous structure is less efficient at restricting the dimensionality of crystal growth.

PB-PEO Templated Titania Films. In-situ thermal ellipsometry of cubic PB-PEO-templated titania films shows the influence of the template during synthesis and is compared directly with in-situ SAXS results, Figure 17. The ellipsometry profile is quite different from that of Pluronic-templated titania with template removal, beginning above 260 °C, causing a large contraction in the thickness of the film but also an increase in the composite index of refraction. The contraction profile in ellipsometry and SAXS data are nearly identical with a temperature shift caused by differences in the experimental setup (and possibly support effects due to the difference in thickness and flexibility of the silicon support, see Experimental Section for details). SAXS data reveals a characteristic distance of 14.3 nm in the direction normal to the film surface, significantly contracted (after aging at 130 °C for 20 h) from the characteristic distance of 27 nm in the *XY* directions. Upon calcination, this distance in the normal direction decreases to 8.5 nm at 510 °C, while the characteristic distance in the *XY* directions remains

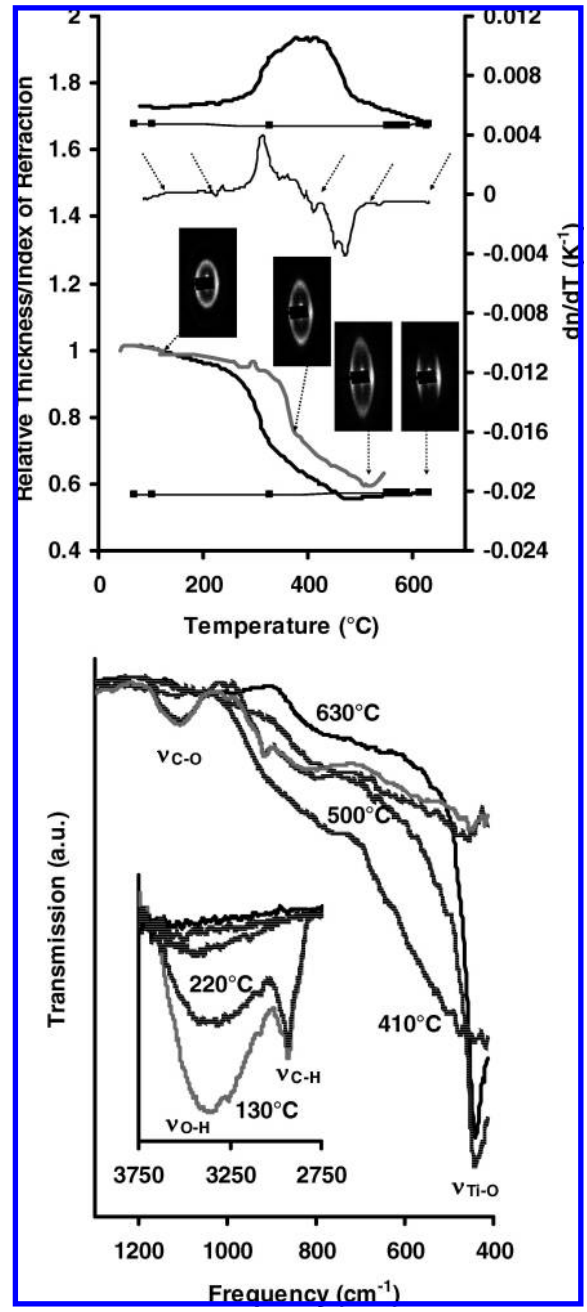

Figure 17. (Top) Relative film thickness and index of refraction and its derivative with respect to temperature measured with (black line) in-situ ellipsometry for a film templated with PB-PEO and heated at 30 °C/min. Contraction of the film normal to the surface determined by (gray line) in-situ SAXS shows near identical behavior with a temperature shift caused by differences in the experimental setup. Arrows on the derivative curve indicate the calcination temperatures for (bottom) ex-situ IR analysis. Initial films thickness was 200 nm.

constant. Beyond this temperature, the periodicity in the [110] axis normal direction is lost due to pore fusion.[61] Ex-situ IR analysis show that both the C−H aliphatic stretch at ∼2930 cm^{-1} and the C−O stretch centered at ∼1100 cm^{-1} disappear over this temperature range (between 220 and 410 °C), indicating that both blocks of the template pyrolyze in this regime. However, at 410 °C, new bands appear around 1615, 1550, and 1415 cm^{-1} (Supporting Information), indicating

(61) Smarsly, B.; Grosso, D.; Brezesinski, T.; Pinna, N.; Boissiere, C.; Antonietti, M.; Sanchez, C. *Chem. Mater.* **2004**, *16* (15), 2948–2952.

Table 1. Summary of Parameters and Their Effect on Calcination and Final Film Processes (↑, small increase; ↑↑, large increase; ↑↑↑, extremely large increase; NC, no change)

	dense films		mesostructured films		
	crystallization	final density	pyrolysis	crystallization	final density
increasing heating rate	↑↑ $T_{max,cryst.}$	↑↑	↑↑ $T_{max,pyr.}$	↑↑ $T_{max,cryst}$	↑↑
increasing H_2O during calcination	↓↓ $T_{max,cryst}$	↓↓	NC[a]	↓↓ $T_{max,cryst}$	↓↓
increasing solution aging	↑ $T_{max,cryst}$	↓	NC	NC	↓
decreasing film thickness	↑ $T_{max,cryst}$	NC	NC	NC	↑
substrate	various	various	various	various	various
increasing mesostructured ordering			NC	↓ dim.[b]	
HCl vapor			↓↓ $T_{max,pyr.}$		↓↓↓

[a] $T_{max,pyr}$is higher for materials calcined under argon due to the absence of O_2. [b] Change in mechanism resulting in an observed reduction of dimensionality in kinetically governing transport processes.

formation of intermediate species, possibly coke-like conjugated carbonaceous species or carboxylates.[62] The presence of intermediate carbonaceous species has been observed in TGA-MS analysis of bulk mesoporous silica materials with some templates[50] and, here, can explain the increase in the composite index of refraction as densification occurs while porosity generation is limited by slow removal of these species. This intermediate species also prevents an accurate analysis of the evolution of pyrolysis, porosity, and crystallization behavior since its optical characteristics cannot be explicitly accounted for. Changes in the FTIR profile showing the development of a broad band at ~443 cm^{-1} at 410 °C and its subsequent sharpening to a feature characteristic of anatase at 500 °C, however, indicate that crystallization is occurring in this range. Finally, bands at ~3370 cm^{-1} show the reduction of O−H stretching as surface OH groups are lost, most predominantly between 130 and 410 °C. The final material exhibits larger pores than the F127-templated material with a slightly lower index of refraction, indicating that the porosity is slightly larger. As such these materials have thicker matrix walls and should exhibit higher mechanical strength and stability.

Conclusions

In-situ thermal ellipsometric analysis is applied to the study of the pyrolysis, crystallization, and sintering of dense and ordered mesoporous titania thin films. This powerful technique is used to elucidate new and fine-scale details on these thermally driven chemical processes that are practically inaccessible via more traditional approaches. Specifically this technique gives access to the index of refraction and film thickness during heating. This information is used to evaluate the evolution of the porosity and material composition as a function of temperature, thus identifying key parameters that effect densification, pyrolysis, crystallization, and sintering. The sum of these processes dictates the final characteristics of prepared thin films and is immensely important in the synthesis and optimization of advanced functional materials based on titania and other thin oxide films. The description of chemical processes occurring inside these materials, including extraction of kinetic parameters, is shown to be accessible via this technique for both the pyrolysis of the template and in the crystallization of the matrix walls. The former reveals a well-behaved first-order mechanism characterized by an activation energy of 124 kcal/mol. The mechanism and kinetic parameters of anatase crystallization are shown to be strongly dependent on the presence of mesoscale ordering with ordered cubic films showing a higher observed activation energy and a lower JMA parameter. The latter indicates a diffusion-limited crystallization process for templated films of lower dimensionality than that of the dense films. Less well-ordered films, prepared from the same template dipping solution but at low relative humidity and characterized by both in-situ ellipsometry and in-situ SAXS, show behavior that is more reminiscent of dense films in terms of the breadth of the crystallization feature despite similar pore volume and pore size distributions to the mesostructured film. In-situ thermal ellipsometry is also used to follow the evolution of the porosity during pyrolysis, crystallization, and sintering. It is used to characterize in detail the influence of the heating schedule, initial film thickness, nature of the substrate, solution aging, presence of water during calcination, nature of the templating agent, and influence of additives in the calcination environment as a function of temperature. These parameters are shown to have unique and often substantial effects on the final film structure, Table 1. In-situ thermal ellipsometry offers detailed insight into the thermally driven chemistry that governs such kinetic processes and thus into the evolution from an assembled film to the final material. Finally, this technique is applicable to the study of a broad range of crystalline, noncrystalline, and hybrid mesoporous materials produced via thermal treatment, by far the most common processing treatment. Such thin film materials encompassing varying structure directing agents, frameworks, and morphologies continue to be a major focus of research for the development of advanced functional materials.

Experimental Section

All products were purchased from Sigma/Aldrich and used as furnished. FTO (fluorine-doped SnO_2) was obtained from ASAHI 100 as a ~100 nm layer deposited on glass substrates 1.1 mm. Titania films were prepared, as reported previously, in the presence of F127 Pluronic block copolymer[19,21] or PB-PEO copolymers as structuring agents by dip coating. Dense films were prepared in the same manner but in the absence of the structure-directing agent. Titania F127 films were prepared from solutions containing molar ratios of $1TiCl_4$:40EtOH:$15H_2O$:0.004F127 using a withdrawal rate of 1.7 mm s^{-1} at a RH less than 15% (dense films were prepared using a withdrawal rate of 0.7 mm s^{-1}). After the dry line reached the bottom of the film, films were placed in a 75% RH environment overnight and subsequently cured at 130 °C for 24 h. Less ordered titania films were prepared using the same initial solution but by dipping at a relative humidity of 5% (held overnight). Controlling the withdrawal rate was used to vary the thickness from 50 to 120 nm for dense films and from 150 to 400 nm for templated films. PB-PEO-based films were prepared from solutions containing molar ratios of $1TiCl_4$:27EtOH:7THF:0.0017PB-PEO (55/45 wt %, 29 800 g mol^{-1}) using a withdrawal rate of 3.2 mm s^{-1} at a RH of 25−30%. For SAXS measurements films were prepared on ultrathin (10−20 μm) silicon wafer substrates. After the dry line reached the bottom of the film, films were placed in a 15% RH environment overnight and subsequently cured at 130 °C for 24 h.

(62) Lichtenberger, J.; Amiridis, M. D. *Catal. Today* **2004**, *98* (3), 447–453.

Ellipsometry measurements were performed on a UV−vis variable-angle spectroscopic ellipsometer (VASE) from Woollam, and data analysis was performed with the WVase32 software. Measurements were fitted over the transparent range for titania (550−1000 nm). A single Cauchy layer was used to model the deposited films, asymmetric optical properties emanating from unidirectional contraction were not observed, and therefore, no correction was applied. Gradients in the thickness were also not observed, as previously reported.[14,33] For in-situ ellipsometric analysis, the ellipsometer was fitted with a home-built covered heating unit connected to a programmable temperature regulator (now being developed in conjunction with SOPRA). Small holes were present to allow a thermocouple and beam access to the sample as well as gas flow. The calcination environment was adjusted by flowing between 1 and 5 L min^{-1} of gas through the sample stage at controlled RH. HCl experiments were conducted by bubbling 1 L min^{-1} through 12 N HCl, while the off gas was ventilated by vacuum (warning: HCl vapor is oxidizing, and necessary precautions should be taken). For environmental porosimetry measurements the ellipsometer was fitted with a small, variable-humidity flow chamber (SOPRA) flushed with 2.5 L of air per min. The humidity was adjusted using a mass flow controller and monitored using a relative humidity probe held in the environmental chamber.[26] In this case, ellipsometry was conducted at room temperature (25 °C) using the adsorption−desorption isotherm of water analyzed with an isotropic inorganic pore contraction model (IIC) and a modified Kelvin equation for ellipsoidal pores.[26]

TEM micrographs were collected using a Philips CM12 transmission microscope. Samples were obtained by scratching the films from the substrate and depositing them on coated copper grids. FT-IR spectrophotometry was conducted using a Nicolet Magna 500 apparatus in transmission mode. Grazing incidence small-angle X-ray scattering (GISAXS) and transmission SAXS were collected using a 16 keV (0.77 Å) beamline of ELETTRA (Trieste, Italy), experimental details of which can be found elsewhere.[14]

Acknowledgment. This material is based upon work supported in part by the National Science Foundation under the International Research Fellowship Program, grant no. (OISE-0505786). The authors also acknowledge funding provided by CNRS and UPMC and assistance at the ELETTRA beamline from Heinz Amenitsch.

Supporting Information Available: Figures and calculation details referenced in the text. This material is available free of charge via the Internet at http://pubs.acs.org.

JA078140X